Brownian Dynamics Theory for Predicting Internal and External Blockages of Tetraethylammonium in the KcsA Potassium Channel

Matthew Hoyles,* Vikram Krishnamurthy,† May Siksik,† and Shin-Ho Chung*

*Research School of Biological Sciences, The Australian National University, Canberra, Australia; and †Department of Electrical Engineering, The University of British Columbia, Vancouver, British Columbia, Canada

ABSTRACT The theory of Brownian dynamics is used to model permeation and the blocking of KcsA potassium channels by tetraethylammonium (TEA). A novel Brownian dynamics simulation algorithm is implemented that comprises two free energy profiles; one profile is seen by the potassium ions and the other by the TEA molecules whose shape is approximated by a sphere. Our simulations reveal that internally applied TEA blocks the passage of K^+ ions by physically occluding the pore. A TEA molecule in the external reservoir encounters an attractive energy-well created by four tyrosine residues at position 82, in addition to all other attractive and repulsive forces impinging on it. Using Brownian dynamics, we investigate how deep the energy-well needs to be to reproduce the experimentally determined inhibitory constant k_i for the TEA blockade of KcsA or the mutant *Shaker* T449Y. The one-dimensional free energy profile obtained from molecular dynamics is first converted into a one-dimensional potential energy profile, and is then transformed into a three-dimensional free energy profile in Brownian dynamics by adding the short-range potential from the channel walls. When converted, the free energy profile calculated from molecular dynamics gives a well-depth of ~10 kT. We systematically alter the depths of the profiles, and then use Brownian dynamics simulations to numerically determine the current versus TEA-concentration curves. We show that the sequence of binding and unbinding events of the TEA molecule to the binding pocket can be modeled by a first-order Markov process. The Brownian dynamics simulations also reveal that the probability of a TEA molecule binding to the binding pocket in KcsA potassium channels increases exponentially with TEA concentration and depends also on the applied potential and the K^+ concentration in the simulation assembly.

INTRODUCTION

Tetraethylammonium (TEA) has long known to be a potent blocker of potassium currents flowing across the cell membrane. TEA has been widely used to separate different components of the membrane currents and to probe the dynamics of ion permeation across potassium channels. Many potassium channels are blocked by TEA molecules applied to the internal (1) and external sides of the membrane (2,3). Different K^+ channels display different sensitivity to external TEA. For example, the inhibitory constant k_i for the *Shaker* K^+ channel is 27 mM, but its TEA affinity increases drastically when the threonine residue at position 449 is substituted with the tyrosine or phenylalanine residue (3,4). In KcsA and Kv2.1, where four tyrosine residues (at position 82 or 380), located just external to the selectivity filter, form a binding pocket for TEA, the current is halved when its concentration reaches between 1.7 and 4.5 mM (5–8). The external TEA affinity in KcsA is drastically reduced when tyrosine at position 82 is substituted with nonaromatic residues, such as cysteine or threonine (5). The precise mechanism that influences TEA potency in different channels and the structural basis of the forces that stabilize a TEA molecule in the outer vestibule are not fully understood.

The one-dimensional free energy profile computed using molecular dynamics shows that a TEA molecule sees a shallow attractive potential well as it enters the binding pocket (9,10). This well extends ~6 Å in the direction normal to the membrane, and its deepest position, located outside of the selectivity filter, is ~4.45 kcal/mol or 7.5 kT (1 kcal/mol equals 1.69 kT at 298°C) (9). From steric considerations, it is postulated that the stabilizing effects between the aromatic rings of the tyrosine residues and a TEA molecule arise from hydration rather than electrostatic forces (9,10). On the other hand, using the nonsense suppression method in the mutant *Shaker*, Ahern et al. (11) provide experimental and computational evidence supporting the idea that external TEA blockade in *Shaker* arises, in large part, from a cation-π electron interaction between the aromatic ring of the tyrosine residues at position 449 and a quaternary ammonium ion.

The picture emerging from these studies is that in the KcsA and *Shaker* potassium channels, a TEA molecule physically occludes the pore when it is sequestered by four tyrosine residues located just external to the selectivity filter. In the Kv2.1 channel, which is a slowly inactivating delayed rectifier responsible for repolarization of the action potential, evidence suggests that current block by external TEA may hinge on several other factors. For example, TEA is ineffective in blocking Na^+ currents flowing across this channel, in the absence of K^+ (6). The substitution of the

---

Submitted June 13, 2007, and accepted for publication August 28, 2007.

Address reprint requests to Shin-Ho Chung, E-mail: shin-ho.chung@anu.edu.au.

Editor: Gregory A. Voth.

© 2008 by the Biophysical Society

0006-3495/08/01/366/13 $2.00

doi: 10.1529/biophysj.107.115139

tyrosine residues at position 380 (corresponding to position 449 in *Shaker*) with cysteines has relatively small effect on TEA block; this mutation shifts the inhibitory constant from 3 to 9 mM (12). Thus, the stabilization of TEA in the external vestibule is influenced by, among other factors, the conformation of the vestibule, the electrostatic milieu near the binding pocket, and the occupancy state of the selectivity filter. It is possible that, in the course of a prolonged activation of the channel, TEA efficacy undergoes dynamic changes, as does the conformation of the external vestibule (13,14) and of the selectivity filter (15).

The aim of this article is to show that Brownian dynamics (BD) simulations can reveal further insights into the action of internally and externally applied TEA on the permeation dynamics. The BD simulations are run for a period long enough to study the effects of TEA in the simulation assembly on the conductance properties of the KcsA K^+ channel. The ability to run simulations over a period long enough to determine statistically consistent estimates of the current flow across ion channels is a distinct advantage of BD over molecular dynamics. This is achieved by making two approximations. First, BD assumes a fixed protein structure, so that the explicit dynamics of protein molecules are not simulated. Second, in BD, the dynamics of water molecules are not simulated. Instead, the net effect of incessant collisions between water molecules and ions, or water molecules and TEA molecules, are represented as frictional and random forces. These random forces are modeled as Brownian motion based on a functional central limit theorem approximation. This means that the hydration structure of molecules in the simulation assembly, or the attractive interaction between molecules via hydration forces, are not taken into account.

The forces arising from the interaction between a charged TEA molecule and the quadrupolar moment of the aromatic ring are computed from the three-dimensional free energy profile a TEA molecule encounters as it moves from the outer vestibule toward the selectivity filter of the KcsA channel. As described in Appendix 1, the one-dimensional free energy profile, taken from molecular dynamics calculations (9), is converted into a one-dimensional potential energy profile to be used in BD simulations. The shape of the one-dimensional potential energy profile for TEA remains virtually identical to that of the one-dimensional free energy profile but its depth increases slightly once these conversions are made.

With this modification of the free energy profile, we carry out BD simulations of the KcsA potassium channel with KCl ions and TEA molecules both present. In this novel BD algorithm, the motion of TEA is influenced by the electrostatic, random, and frictional forces, as well as the attractive force arising from its interaction with four tyrosine residues just outside of the selectivity filter. This free energy profile, invisible to other charged particles in the simulation assembly, is in turn modulated by the locations of resident K^+ ions in the selectivity filter. With these simulation techniques, we uncover several additional insights into the mechanisms of internal and external TEA blockade. First, we reproduce the macroscopically observed binding affinity of TEA through the fundamental processes operating in electrolyte solutions. By constructing the current-TEA-concentration curves using different energy profiles with different well-depths, we are able to determine the binding energy between TEA and the channel to account for the experimentally observed inhibitory constant k_i. Second, we show how the inhibitory constant is pronouncedly influenced by the applied membrane potential and ionic concentrations of K^+ ions in the reservoirs. Such dynamic interactions arising from the presence of many particles cannot be revealed from a static profile of potential of mean force. Third, with the BD simulation technique, we have been able to investigate the kinetics of TEA binding and unbinding. We show that they follow a first-order Markovian process, and construct the transition probability matrices at various applied potentials and ligand concentrations. The opening and closing of a single channel is governed by a Markovian process (16,17). Within each brief open episode in the presence of TEA, the channel is blocked and unblocked at a fast timescale, according to another Markovian process. Finally, we show how the channel is blocked by TEA applied to the internal side of the membrane.

METHODS

Channel models

The channel structure we use for this study is the same as that used in previous BD simulations of the KcsA potassium channel (18). The model channel is based on the crystal structure of Doyle et al. (19) with the pore expanded at the internal end of the channel using a cylindrical repulsive potential in molecular dynamics to have a radius of 5 Å. As described previously, the selectivity filter is also expanded slightly such that the minimum radius is 1.4 Å. The full charges of $-e$ and $+e$ are assigned to D_{80} and R_{64} located at the extracellular aspect of the channel, whereas a partial charge of $-0.5e$ and $+0.5e$ is assigned to the ionized pair, E_{118} and R_{117}, guarding the intracellular gate. One unpaired arginine residue (Arg_{27}) and the two pairs of ionizable residues, namely, Glu_{51}/Arg_{52} and Glu_{71}/Arg_{89}, are kept neutral, for the reasons detailed in Chung et al. (23). For this study, we selected this model, among several other permeable forms of KcsA (see, for example, (18)), as it more accurately replicates the experimental data, such as the observed current-voltage-concentration profiles.

Brownian dynamics

The algorithm for performing BD simulations is conceptually simple. The position and velocity of each individual ion in and around the ion channel evolves according to a continuous time stochastic dynamical system. The position $\mathbf{x}_t^i$ and velocity $\mathbf{v}_t^i$ of the i^{th} ion at time t with mass m and charge q located at a given position are determined by the force acting on it and are computed by integrating the equation of motion, known as the Langevin equation, a stochastic version of Newton's equation of motion. Thus,

$$\mathbf{x}_t^{(i)} = \mathbf{x}_0^{(i)} + \int_0^t \mathbf{v}_\tau^{(i)} d\tau, \qquad (1)$$

$$m\mathbf{v}_{\mathrm{t}}^{(\mathrm{i})} = m\mathbf{v}_{0}^{(\mathrm{i})} - \int_{0}^{\mathrm{t}} m\gamma(\mathbf{x}_{\tau}^{(\mathrm{i})})\mathbf{v}_{\tau}^{(\mathrm{i})}d\tau + \int_{0}^{\mathrm{t}} F_{\lambda}^{(\mathrm{i})}(\mathbf{x}_{\tau})d\tau + \int_{0}^{\mathrm{t}} b(\mathbf{x}_{\tau}^{(\mathrm{i})})d\mathbf{w}_{\tau}^{(\mathrm{i})}. \tag{2}$$

Here, $m\gamma$ is the frictional coefficient and the process $\{\mathrm{w}_{\tau}^{(\mathrm{i})}\}$ denotes a three-dimensional zero-mean Brownian motion, which is component-wise independent. The constant b is related to the friction coefficient by $b^2(\mathrm{x}_{\tau}^{(\mathrm{i})}) = 2m\gamma(\mathrm{x}_{\tau}^{(\mathrm{i})})kT$. Here, λ denotes experimental conditions, such as external applied voltage and ionic concentrations, and F_λ denotes systematic electrostatic forces. Thus, there are two main sources of the forces influencing the motion of ions that result in the channel current. These are the stochastic force and electric force. The former arises from the effects of incessant collisions between ions and water molecules. As a result of such bombardments, the motion of an ion is retarded by the friction term, and it undergoes random fluctuations from an equilibrium position via the Brownian motion term. The Langevin equation is often presented as

$$m\frac{d\mathbf{v}_{\mathrm{t}}^{(\mathrm{i})}}{dt} = -m\gamma(\mathbf{x}_{\mathrm{t}}^{(\mathrm{i})})\mathbf{v}_{\mathrm{t}}^{(\mathrm{i})} + F_{\lambda}^{(\mathrm{i})}(\mathbf{x}_{\mathrm{t}}) + b(\mathbf{x}_{\mathrm{t}}^{(\mathrm{i})})\mathbf{e}_{\mathrm{t}}^{(\mathrm{i})}, \tag{3}$$

where $\mathbf{e}_{\mathrm{t}}^{(\mathrm{i})}$ denotes continuous-time white noise.

Ions are initially assigned random positions with a specified mean concentration and Boltzmann-distributed velocities within cylindrical reservoirs of 30 Å radius attached to either end of the channel that mimic the intracellular and extracellular space. We calculate the total force acting on each ion in the assembly and then determine new positions for the ions a short time later using an algorithm described elsewhere (20–22). A multiple time-step algorithm is used, where a time-step of $\Delta t = 100$ fs is employed in the reservoirs and 2 fs in the channel where the forces change more rapidly.

The electrostatic forces F_λ acting upon the ions are calculated by solving Poisson's equation using a boundary element method (24). To do this we assign a dielectric constant of $\epsilon_{\mathrm{p}} = 2$ to the protein and membrane and $\epsilon_{\mathrm{w}} = 60$ to the water inside the channel as in previous BD studies of the KcsA channel (18). Since calculating the electric forces at every step in the simulation is very time-consuming, we store precalculated electric fields and potentials due to one- and two-ion configurations in a system of lookup tables and interpolate values for the given ion positions from these during the simulation (21).

For this purpose, the total electric potential ϕ_{i} encountered by a charged particle i (including TEA molecules) is decomposed into four components:

$$\phi_{\mathrm{i}} = \phi_{\mathrm{X,i}} + \phi_{\mathrm{S,i}} + \sum_{\mathrm{j}\neq\mathrm{i}}(\phi_{\mathrm{I,ij}} + \phi_{\mathrm{C,ij}}). \tag{4}$$

The four terms on the right-hand side of Eq. 4 are, respectively, the external potential due to the applied field and fixed charges in the protein and charges induced by these, the self-potential due to the surface charges induced by the ion i on the channel boundary, the image potential due to the charged induced by the ion j, and the Coulomb potential due to the ion j. The first three potential terms are stored in, respectively, three-, two-, and five-dimensional tables.

The short-range forces are used to keep the ions and TEA molecules in the simulation assembly and also to mimic other interactions between charged particles that are not included in the Coulomb interaction. To prevent charged particles from leaving the system, a hard-wall potential is activated when they are within one ionic radius of the reservoir boundaries. Thus, a particle colliding with the boundary of the reservoir is elastically scattered. For the ion- or TEA-wall interaction U^{IW}, we use the $1/r^9$ repulsive potential

$$U^{\mathrm{IW}}(r) = \frac{F_0}{9}\frac{(R_{\mathrm{i}} + R_{\mathrm{w}})^{10}}{(R_{\mathrm{c}}(z) + R_{\mathrm{w}} - a)^{9}}, \tag{5}$$

where R_{i} is the radius of ions or TEA, R_{w} is the radius of the atoms lining the protein wall, $R_{\mathrm{c}}(z)$ is the radius of the channel as a function of the z coordinate, and a is the ion's (or TEA molecule's) distance from the z axis. We use $F_0 = 2 \times 10^{-10}$ N in Eq. 5, which is estimated from the ST2 water model used in molecular dynamics (25). At short-ranges, the Coulomb interaction between two charged particles is modified by adding a potential U^{SR}, which replicates effects of the electron clouds and hydration. Molecular dynamics simulations show that the hydration forces between two charged particles add further structure to the $1/r^9$ repulsive potential due to the overlap of electron clouds in the form of damped oscillation (26,27). This additional potential is incorporated in our Brownian dynamics such that the radial distribution functions derived from BD simulations replicate those found in molecular dynamics simulations. For further details of the implementation of short-range forces, see Corry et al. (28).

Tetraethylammonium in the BD algorithm

Ideally, each TEA molecule should be represented as a rigid oblate shape, a spheroid generated by the revolution of an ellipse, with the long and short axes equal to 4.6 and 2.3 Å. For this study, we use a simple, spherical model of TEA with the radius of either 2.3 Å (for externally applied TEA) or 3.4 Å (for internally applied TEA). The molecular weight and diffusion coefficients used for the spherical TEA model are, respectively, 130.25 and 0.87×10^{-9} m^2 s^{-1} (29).

Crouzy et al. (9) calculated a free energy profile encountered by a TEA molecule as it moves from the external reservoir toward the selectivity filter (Fig. 1, *top*). To convert this one-dimensional free energy profile, calculated using CHARMM, to a three-dimensional free energy profile that can be incorporated into the BD algorithm, we first fit an analytical function to the

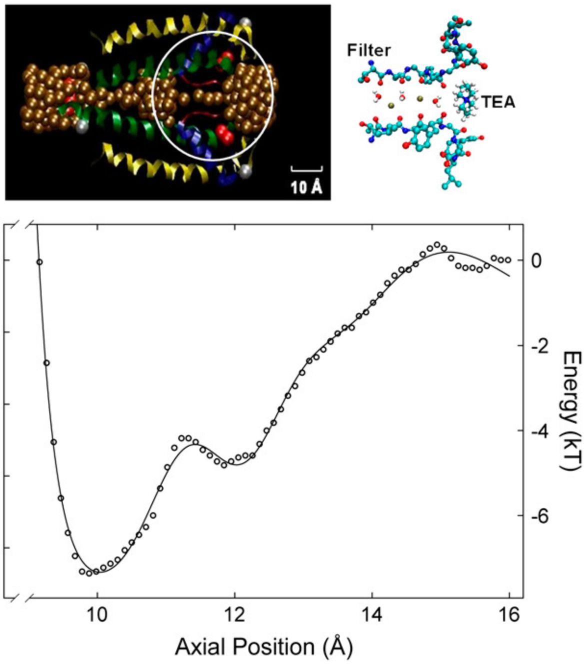

FIGURE 1 Model potassium channel. (*Top*) Two of the four subunits of the full experimentally determined KcsA protein are represented as ribbons. Water molecules are shown in gold. The circled region of the protein, containing the selectivity filter is enlarged on the right-hand side and shown in a stick-and-ball model, together with three water molecules and 2 K$^+$ ions (*gold*). In simulations, each TEA molecule in the external reservoir is represented as a sphere with radius of 2.3 Å, and that in the internal reservoir as a sphere with radius of 3.2 Å. (*Bottom*) The one-dimensional free energy profile obtained by Crouzy et al. (9) replotted (*open circles*). The digitized data points are fitted with three analytical functions (*solid line*). The origin of the profile is at the center of the mass of the selectivity filter.

profile obtained by Crouzy et al. (9) (Fig. 1, *bottom*, *open circles*). The digitized points are fitted with the sum of three simple algebraic functions:

$$f_1(z) = A_1\epsilon_1\left[\left(\frac{\sigma_1}{z-r_1}\right)^{12} - \left(\frac{\sigma_1}{z-r_1}\right)^{2}\right], \qquad (6)$$

$$f_2(z) = -A_2\epsilon_2\exp\left[-\frac{1}{2}\left(\frac{z-r_2}{\sigma_2}\right)^{2}\right]\sin\left[\pi\left(\frac{z-r_2}{\sigma_2}\right)\right], \qquad (7)$$

$$f_3(z) = \epsilon_3\exp\left[-\frac{1}{2}\left(\frac{z-r_3}{\sigma_3}\right)^{2}\right]. \qquad (8)$$

The coefficient A_1 is chosen such that $f_1(z) = -\epsilon_1$ at the minimum. Similarly, A_2 is chosen such that $f_2(z) = \pm\epsilon_2$ at the maximum and minimum. The parameters are adjusted to a least-squares fit using the Levenberg-Marquardt method (30). The final parameters used to fit the experimentally determined free energy profile, shown in Fig. 1, *bottom* (*solid line*), are: $\epsilon_1 = 4.21$ kcal/mol; $\sigma_1 = 4.09$ Å; $r_1 = 5.06$ Å; $\epsilon_2 = 0.47$ kcal/mol; $\sigma_2 = 1.06$ Å; $r_2 = 11.71$ Å; $\epsilon_3 = 1.33$ kcal/mol; $\sigma_3 = 1.06$ Å; $r_3 = 14.91$ Å.

We then transform the analytical one-dimensional free energy profile G_{1d} into a three-dimensional free energy profile G_{3d}, taking into account the effective cross-sectional area at each z position. This conversion is done by first obtaining a one-dimensional potential profile U^{PMF} and then adding to it the short-range potential which represents repulsion from the channel wall. The relationship between the free energy in one-dimension G_{1d} and that in three-dimension G_{3d} is given in Appendix 1. The depth of the well of the one-dimensional potential profile U^{PMF} is ~2.5 kT deeper than the free energy profile in one-dimension G_{1d}.

The position of the center of mass of the selectivity filter, which is taken as the origin of the z axis in Fig. 1, is at $z = 15.1$ Å in our coordinate system (where $z = 0$ is taken to be at the midway between the two ends of the channel). The three-dimensional free energy profile G_{3d} is spliced onto the usual BD force field using a reference potential $U^{REF}(z)$. This potential is used along the z axis in the region ($z = 24.1$ to 31.1 Å) with two K^+ ions in the selectivity filter of the channel to reproduce as closely as possible the conditions of the MD simulation. Except for short-range potentials, all electrostatic effects, such as direct and indirect image effects of the channel dielectric boundary, are included. The reference potential is then subtracted to avoid double counting of potentials already included from the molecular dynamics free energy profile. The positions of the two K^+ ions in the selectivity filter are allowed to vary to minimize the total energy. These two positions range from $z = 9.55$ to 9.71 Å, and from $z = 16.47$ to 16.66 Å. This reference potential is then subtracted from the BD potential where the potential profile U^{PMF} is added. When the configuration of ions is different, these differences are taken into account by the resulting change in the BD potential.

We employ, when needed to maintain low concentrations of TEA in the external reservoir, the grand canonical Monte Carlo method (31). The effective volume of each reservoir in our simulation system is 8.7×10^{-26} m^3. Since placing one molecule in the reservoir will bring its concentration to ~20 mM, we make use of this method to maintain a low TEA concentration, rather than increasing the size of the reservoirs. The technical details of implementing the grand canonical Monte Carlo method are given in Corry et al. (32).

RESULTS

Blockade of KcsA by internally applied TEA

Our BD simulations reveal that internally applied TEA acts by physically occluding the pore. BD simulations are carried out with either one or more TEA molecules in the internal vestibule, and 16 K^+ and 16 Cl^- ions in each reservoir. In these simulations, the free energy profile calculated from molecular dynamics is not included. Yellen et al. (2) identified an amino-acid residue in the *Drosophila Shaker* channel that influences the affinity for TEA applied intracellularly. The current in the wild-type *Shaker* (*ShIR*) is halved when 1 mM TEA is applied on the internal face of the channel. Substitution of threonine residue at position 441 with serine drastically alters sensitivity to internal TEA. The sensitivity of the T441S mutant channel to TEA is reduced by an order of magnitude compared to the wild-type *ShIR* channel. In the KcsA channel, however, sensitivity to internal TEA is relatively low (5), and no TEA binding site in the inner vestibule, equivalent to position 441 located along the inner vestibule *Shaker* or to position 82 in the outer vestibule of KcsA, has been identified. For this reason, we do not use any special energy function for the intracellularly applied TEA.

As a TEA molecule carries one positive charge, one additional Cl^- for each molecule is placed in the internal reservoir to render the solutions in the reservoir electroneutral. When one TEA molecule is placed in the reservoir, its concentration becomes 20 mM. The concentration of K^+, unless noted otherwise, is kept constant at 300 mM. A TEA molecule enters the intracellular mouth of the channel quickly, attracted by the energy-well created by four glutamate residues, E_{118}. With low applied potentials, a TEA molecule that manages to enter the channel stays mainly in the energy-well in the intracellular gate, as shown in the dwell histogram shown in Fig. 2 *A*. With high applied potentials, however, the resident TEA molecule moves further inside the channel, and spends part of the time near the entrance of the selectivity filter (Fig. 2, *B* and *C*). Because of its large size, a TEA molecule is unable to pass through the selectivity filter. In the presence of a TEA molecule anywhere along the ion-conducting pathway, the channel is effectively blocked, as no K^+ ions can pass around this bulky molecule.

The amount of blocking depends both on the applied potential and TEA concentration. In Fig. 3 *A*, the percentages of the currents relative to the control currents are plotted against applied potentials with the TEA concentrations of 20, 40, and 100 mM. With the concentration of 20 mM, we see that TEA blockade is weakly voltage-dependent when the applied potential is low, but becomes strongly voltage-dependent at higher applied potentials. With higher TEA concentrations, however, the currents relative to the control currents rapidly decline with an increase in the applied potential. The inhibitory constant for the internal TEA block we derive is 40 mM at 130 mV and 20 mM at 170 mV. The results described thus far are obtained from simulations, in which a TEA molecule is represented as a sphere with a radius of 3.4 Å. The minimum and maximum radii of a TEA molecule are, respectively, 2.3 and 4.6 Å, and its volume average is 3.4 Å. To test the sensitivity of the results on the radius of sphere used, we repeat one set of simulations as

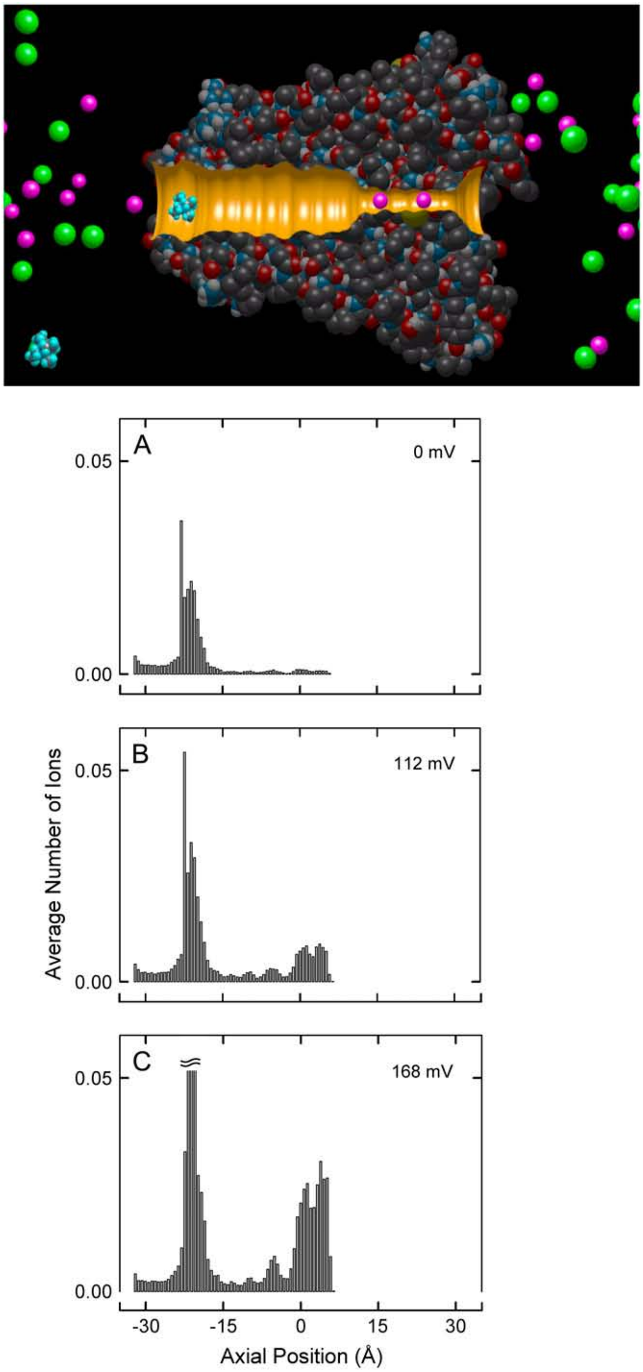

FIGURE 2 Dwell histograms of internal TEA molecules in the channel. The inset shows the simulation assembly consisting of the KcsA channel at the center and two TEA molecules, K^+ ions (*pink*), Cl^- ions (*green*) in or in the vicinity of the channel. The channel extends from −34.2 Å to +34.2 Å. The channel is divided into 100 thin sections and the average number of TEA molecules in each slice during a simulation period of 0.8 μs is tabulated. The histograms are obtained with an applied potential of 0 mV (*A*), +112 mV (*B*), and +168 mV (*C*).

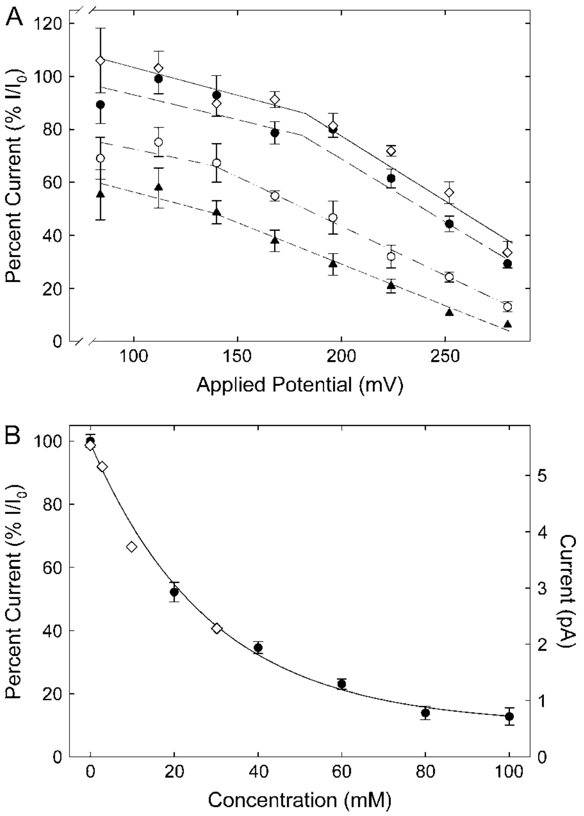

FIGURE 3 Reduction of the currents by internally applied TEA molecules at various applied potentials. (*A*) The current at each applied potential is expressed as a percentage of the current in the absence of TEA. The concentrations of TEA in the internal reservoir are 20 mM (*solid circles*), 60 mM (*open circles*), and 100 mM (*solid triangles*). These three curves are obtained by representing a TEA molecule as a sphere with a radius of 3.4 Å. The measurements are repeated, for the TEA concentration of 20 mM using a sphere with a radius of 2.3 Å (*open diamonds*). In this and all subsequent figures, error bars have a length of 2 SEM, and are not shown when they are smaller than the data points. (*B*) The current-TEA-concentration curve is obtained with the ionic concentration of 150 mM and the applied potential of 224 mV. Superimposed on the simulated data (*solid circles*) are the experimental measurements (*open diamonds*) obtained by Heginbotham et al. (5).

shown in Fig. 3, representing a sphere with a radius of 2.3 Å, instead of 3.4 Å. Using a TEA concentration of 20 mM, we determine the percentage of block, relative to the control, at various applied potentials. The results, shown in the uppermost curve in Fig. 3 *A* (*open diamonds*) may be compared with those obtained with a sphere of a radius of 3.4 Å. There is a small, but consistent, decrease in the effectiveness of internal TEA blockade when the radius representing the molecule is reduced. This is because a K^+ occasionally is able to pass around a TEA molecule blocking the intracellular gate of the channel.

For KcsA, the experimentally determined value of the inhibitory constant k_i for internally applied TEA is 22 mM (5). The applied potential and ionic concentration used to determine this constant are, respectively, 200 mV and 100 mM. To check how closely our results match the experimental observations, we construct a current-TEA-concentration for the ionic concentration curve, using the K^+ concentration of 150 mM and the applied potential of 224 mV. The experimental measurements (*open diamonds*) are superimposed on the curve derived from BD simulations (*solid circles*) in Fig. 3 *B*.

Blockade of KcsA by externally applied TEA

A TEA molecule in the external vestibule of KcsA sees an attractive potential well created by four tyrosine residues at position 82, located just outside the selectivity filter. Molecular dynamics calculations reveal that this well extends ~6 Å along the z axis, as shown in Fig. 4. The one-dimensional free energy profile (*dashed line*) obtained by Crouzy et al. (9) is converted to one-dimensional potential energy (*solid line*). The resulting profile, once the free energy profile has been converted into the potential energy profile to be used in BD simulations, has a shape virtually identical to the free energy profile. The well starts at $z = 30$ Å (or $z = 15$ Å from the center of mass of the selectivity filter) and reaches its deepest point at $z = 24.44$ Å. The depth of the potential well at this position is 10 kT, ~2.5 kT deeper than the one-dimensional free energy profile. We incorporate this potential energy into the BD algorithm, taking into account the short-range repulsive forces.

Using this profile, with the well-depth of ~10 kT at $z = 24.44$ Å, we construct the current-TEA-concentration profiles at three different values of applied potentials. For all potentials, the currents decrease exponentially as a function of the TEA concentration, as illustrated in Fig. 5. The inward currents are reduced to 50% of the control value at the TEA concentrations of 10, 17, and 24 mM when the applied potentials are, respectively, −224, −168, and −112 mV (inside negative with respect to outside). Thus, the magnitude of attenuation of the inward current by TEA depends on its concentration as well as the applied potential. The inhibitory constants k_i we obtain at all applied potentials are higher than the experimentally determined value, which is 3.2 mM at 200 mV (5).

How deep does the energy-well have to be to replicate the experimentally determined inhibitory constant? We systematically change the depth of the potential energy profile by multiplying the original curve by 0.9, 1.1, 1.2, 1.3, and 1.4 and then construct the current-concentration curves with the applied potential of −168 mV. The corresponding well-depths at $z = 24.44$ Å are, respectively, 9, 11, 12, 13, and 14 kT, as shown in Fig. 6 *A*. The family of current-concentration curves obtained with five different profiles of differing well-depths are displayed in Fig. 6 *B*. The curve obtained with the original profile (reproduced from Fig. 5) is included here for completeness. Each set of data points is fitted with an exponential curve. The half saturation values k_i obtained from the current-concentration curves are: 9.6, 5.4, 3.1, and 2.0 mM when the original profile is multiplied by 1.1, 1.2, 1.3, and 1.4, respectively.

We next explore how external TEA blockade is influenced by the applied potential. With a fixed TEA concentration of 3.2 mM TEA, and with the potential profile with the well-depth of 13 kT, we determine the currents flowing across the

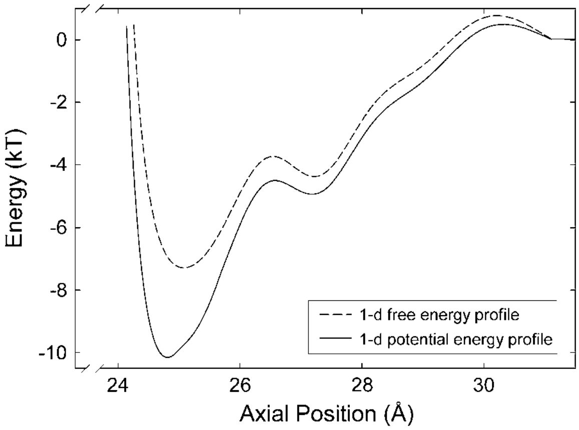

FIGURE 4. Conversion of the one-dimensional free energy profile to a one-dimensional potential energy profile. The analytical function fitted to the experimentally determined free energy profile (*solid line*), as shown in Fig. 1, is used to derive an equivalent one-dimensional potential energy profile (*dashed line*) to be used in Brownian dynamics. The theoretical basis for this relationship is given in Appendix 1. When a short-range force is added to this potential profile, it becomes equivalent to a three-dimensional free energy profile that can be incorporated into the Brownian dynamics algorithm.

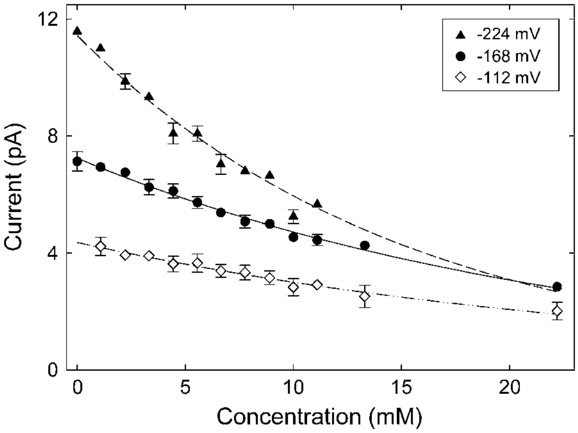

FIGURE 5 The current-TEA-concentration curves. The one-dimensional potential energy profile shown in Fig. 4, after adding a short-range force, is incorporated into the BD algorithm and the current flowing across the channel at different TEA concentrations is determined under the applied potentials of −224 mV (*solid triangles*), −168 mV (*solid circles*), and −112 mV (*open diamonds*). The data points are fitted with the exponential function of the form: $I = I_0 \exp(-bc)$, where I_0 is the control current in pA and c is the TEA concentration in mM. The values of I_0 and b for the three curves are: 11.4 and 0.065 for −224 mV; 7.2 and 0.043 for −168 mV; and 4.36 and 0.037 for −112 mV.

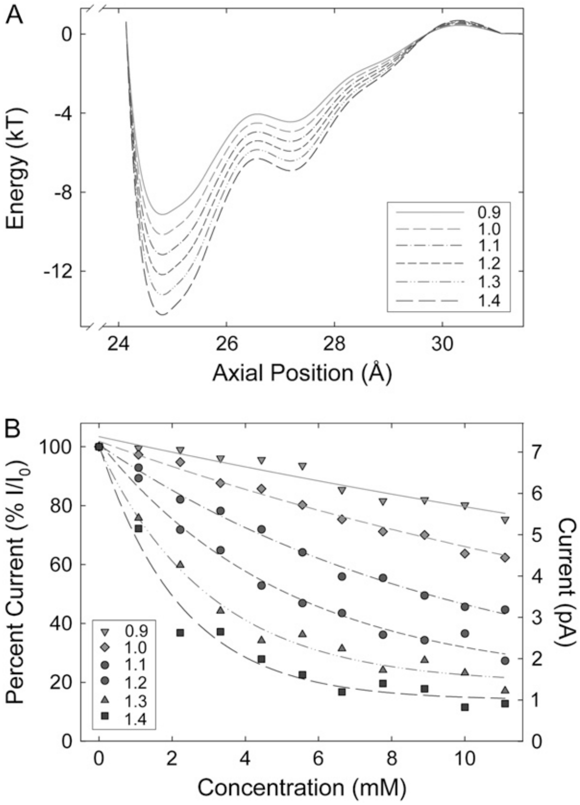

FIGURE 6 The current-TEA-concentration curves with varying well-depths. (*A*) The depth of the three-dimensional free energy profile is systematically altered by multiplying the one-dimensional potential energy profile shown in Fig. 4 by 0.9, 1.0, 1.1, 1.2, 1.3, and 1.4. The depth of the original potential energy profile at $z = 24.44$ Å from the center of the mass of the selectivity filter is 10.0 kT. (*B*) For each profile shown in panel *A*, the current-TEA-concentration curves are constructed. The free energy profiles used for simulations are indicated in the inset. The parameters b of the exponential function, $I = a\exp(-b(c))$, used to fit the data points from the top to bottom curves, are 0.026, 0.047, 0.099, 0.194, 0.328, and 0.446.

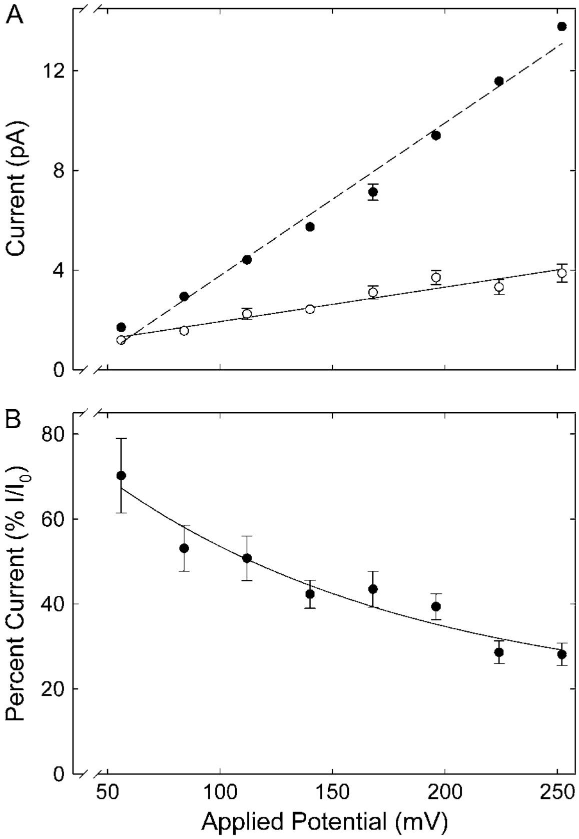

FIGURE 7 Reduction of the currents at different applied potentials. The TEA concentration in the external reservoir and the depth of the well seen by a TEA molecule at $z = 24.44$ Å are kept constant at 3.2 mM and 13 kT, respectively. (*A*) The current increased linearly with an increasing applied potential in the absence (*solid circles*) and presence (*open circles*) of TEA. (*B*) The percentage of the current relative to the control current decreases steadily as the applied potential is increased.

channel at various applied potentials. The current-voltage relationships obtained with (*open circles*) and without TEA (*solid circles*) in the external reservoir are illustrated in Fig. 7. The currents under both conditions increase linearly with the applied potentials. The percentage of currents attenuated by 3.2 mM TEA in the external vestibule, however, changes from 70% of the control current at the applied potential of −56 mV to 30% at −256 mV. Thus, for a fixed concentration, external TEA blockade becomes progressively more effective as the driving force is increased.

The inhibitory constant k_i also depends on the concentration of KCl in the outer reservoir. We construct, in Fig. 8, the current-KCl-concentration curves with (*open circles*) and without TEA (*solid circles*) in the external reservoir. The TEA concentration and the depth of the potential profile are, respectively, 3.2 mM and 13 kT, as used for the simulations illustrated in Fig. 7. The current under both conditions increases rapidly with an increasing ionic concentration and then saturates, leading to current-concentration relationships of the Michaelis-Menten form. The percentage of attenuation caused by TEA of a fixed concentration decreases as the ionic concentration is increased, as shown in Fig. 8 *B*. For example, the current in the presence of 3.2 mM TEA is reduced to 31% of the control value when the ionic concentration in the reservoir is 75 mM. The corresponding value at the KCl concentration of 900 mM is 60%.

The best agreement between the experimentally determined k_i value for KcsA (5) and simulation results is obtained when the depth of the potential profile seen by TEA is assumed to be 13 kT. In Fig. 9, we plot the current-TEA-concentration curve obtained with the driving force of 196 mV and the ionic concentration in both reservoirs of 150 mM. Superimposed on the simulated data (*solid circles*) are the measurements obtained by Heginbotham et al. (5) (*open diamonds*). These experimental data points are obtained with the ionic concentration of 100 mM and the applied potential of 200 mV. To replicate the k_i value for the mutant *Shaker* T449Y (4), the depth of the free energy-well needs to be increased to ∼15 kT.

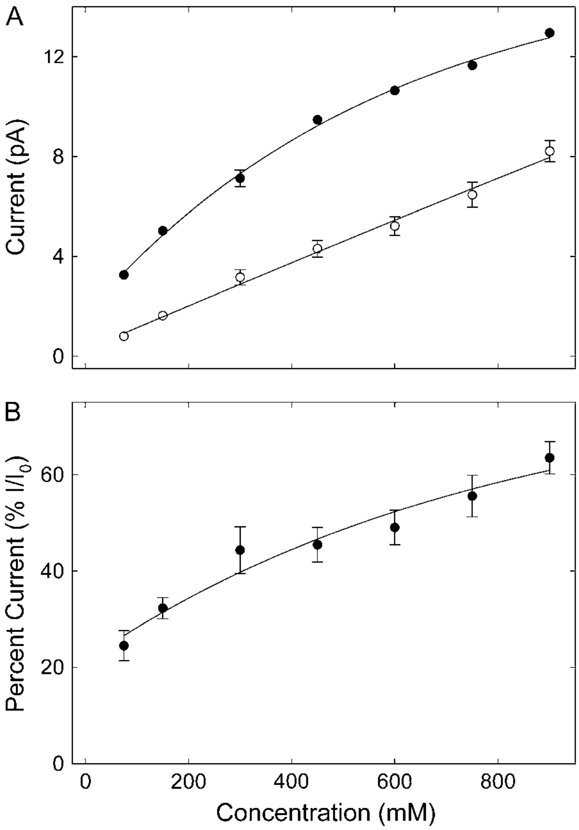

FIGURE 8 Effectiveness of internal TEA at different K$^+$ concentrations. The TEA concentration in the external reservoir and the well-depth seen by a TEA molecule at $z = 24.44$ Å are kept constant at 3.2 mM and 13 kT, respectively. (*A*) The currents increase both in the absence (*solid circles*) and presence (*open circles*) of TEA increase monotonically as the K$^+$ concentration is increased from 75 mM to 900 mM. (*B*) The percentage of the current relative to the control current increases as the K$^+$ concentration is increased.

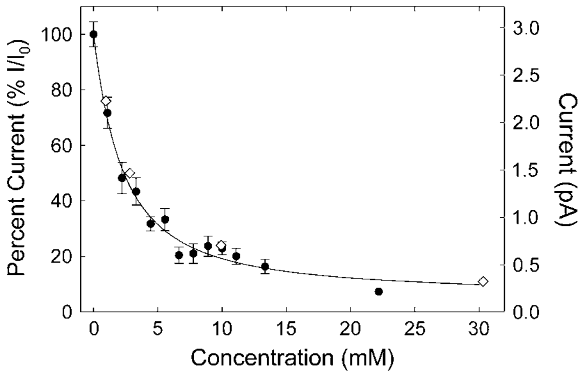

FIGURE 9 Comparison with the experimentally determined inhibitory constant. The currents derived from BD simulations (*solid circle*) at various TEA concentrations are compared with those determined experimentally (*open diamonds*) by Heginbotham et al. (5). The applied potential and the ionic concentration used for BD simulations are, respectively, 196 mV and 150 mV. The depth of the energy-well encountered by a TEA molecule is assumed to be 13 kT.

Kinetics of TEA binding and unbinding

The results from BD simulations show that externally applied TEA binds to the binding pocket located just exterior to the selectivity filter and becomes unbound according to a first order Markovian process. We tabulate the time the channel is not blocked by a TEA molecule (off-time) and the time the binding pocket is occupied by a TEA molecule (on-time). A short segment of the on-time and off-time sample path generated from BD simulations is illustrated in Fig. 10. When bound, a TEA molecule effectively blocks the passage of K$^+$ ions. Conduction events occur only when no TEA is in the binding pocket, as indicated with downward marks in Fig. 10. With a 3.2 mM TEA concentration, the channel is blocked and unblocked nearly 300 times in 100 μs, which is usually one digitizing interval of patch-clamp recordings.

To characterize the binding and unbinding processes, we carry out a set of simulations at eight different TEA concentrations under the applied potential of 168 mV and calculate the mean off-time and on-time at each concentration. The depth of the well and ionic concentration used for these simulations are 12.0 kT and 300 mM, respectively. The random sequence of off-times and on-times generated from the BD simulation can be statistically modeled as a first-order two-state continuous-time Markov process with a transition rate matrix denoted $Q(c)$ as a function of the TEA concentration c. We statistically validate whether or not the binding or unbinding process obeys a first-order, continuous-time, Markov process. One way to demonstrate this would be to construct an interval histogram, which will be distributed as a single exponential function if the process is a first-order Markovian. That is, the random sequences of on-times or off-times denoted t for a given concentration c have an exponential probability distribution function of the form 1-exp($-t/\tau_{\mathrm{ON}}(c)$) and 1-exp($-t/\tau_{\mathrm{OFF}}(c)$), respectively. Here, we use the well-known Anderson-Darling statistical test (33) to determine whether the small number of random sequence of on- and off-intervals we obtained from BD simulations can be modeled by an exponential distribution. By using the Anderson-Darling test with a standard significance level of 5%, we find that the hypothesis that the sequence of

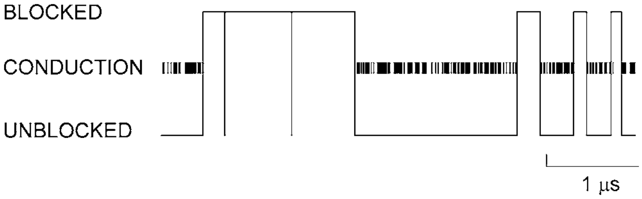

FIGURE 10 Sequence of TEA binding and unbinding. A short segment of the TEA binding and unbinding process is illustrated. The sequence is governed by the first-order Markov process, and the conduction events take place only when a TEA molecule is not in the binding pocket, as indicated by downward marks.

off-times and on-times generated by BD simulation at various TEA concentrations is exponentially distributed, cannot be rejected. Thus, the random sequence of on-times (blocking of the channel by TEA) and off-times (unblocking of the channel) obtained from BD simulations forms a two-state continuous-time Markov chain holds.

The mean off-times $\tau_{\mathrm{OFF}}(c)$ and on-times $\tau_{\mathrm{ON}}(c)$ for different concentrations c in mM computed from the data is shown in Fig. 11 *A*. The figure shows that the time the molecule stays bound to the channel at different TEA concentrations, τ_{ON}, remains fairly constant (*open circles*), whereas the time channel remains unbound to the molecule, τ_{OFF}, decreases as the TEA concentration in the reservoir increases (*solid circles*).

We now show that the elements of the transition rate matrix $Q(c)$ behave as exponential functions of the concentration c. Thus, the binding and unbinding of TEA from BD simulations has a compact statistical representation. By relating the continuous-time transition rate matrix $Q(c)$ to the TEA concentration c, we give an explicit characterization of the stationary distribution of the Markov chain and hence the average channel current versus concentration c. This allows us to characterize the effect of the blocker on the channel current and in particular give explicit trends as to how the average channel current from BD mimics the actual experimental channel current.

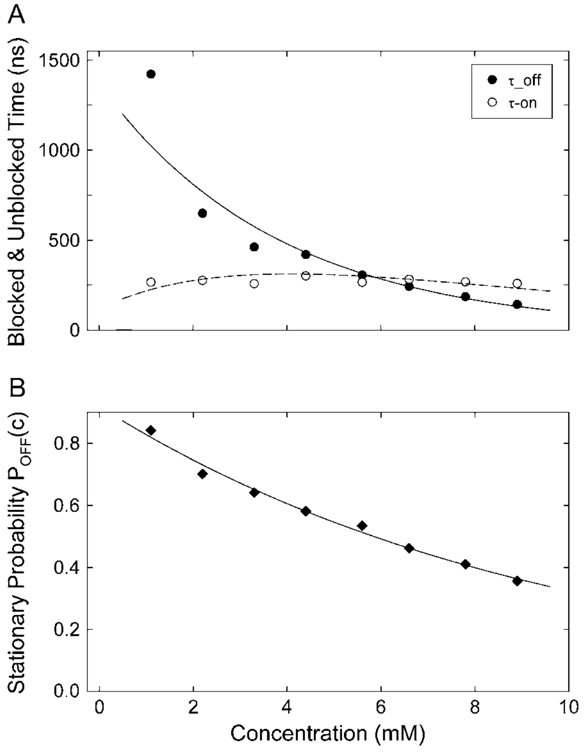

FIGURE 11 Concentration-dependent kinetics of TEA biding and unbinding. (*A*) The mean off-time $\tau_{\mathrm{OFF}}(c)$ (*solid circles*) and the mean on-time $\tau_{\mathrm{ON}}(c)$ (*open circles*) are plotted against the TEA concentration. The on- and off-durations are tabulated during a simulation period lasting 6.4 μs. (*B*) The stationary probability P_{OFF} of a TEA molecule being not bound to the channel is plotted against the TEA concentration.

Let us denote the transition rate matrix of this two-state continuous-time Markov chain as

$$Q(c) = \begin{bmatrix} \dfrac{-1}{\tau_{\mathrm{ON}}(c)} & \dfrac{1}{\tau_{\mathrm{ON}}(c)} \\ \dfrac{1}{\tau_{\mathrm{OFF}}(c)} & \dfrac{-1}{\tau_{\mathrm{OFF}}(c)} \end{bmatrix}. \quad (9)$$

We note here that the transition probability matrix $A(c)$ of the discrete-time Markov chain can be computed from the transition rate matrix $Q(c)$ of the continuous-time Markov chain as $A(c) = \exp(-Q(c)\,\Delta)$, where $\exp(\cdots)$ denotes matrix exponential and Δ is the time discretization interval. However, in the analysis below it is more convenient and intuitive to deal with a continuous-time Markov chain.

Our next task is to model how $Q(c)$ evolves with concentration c. The stationary distribution of the continuous-time Markov chain, which gives the normalized times in which the channel is blocked ($P_{\mathrm{ON}}(c)$) and not blocked ($P_{\mathrm{OFF}}(c)$), is given by the solution of

$$[P_{\mathrm{ON}}(c)\ \ P_{\mathrm{OFF}}(c)]Q(c) = 0, \quad P_{\mathrm{ON}}(c) + P_{\mathrm{OFF}}(c) = 1. \quad (10)$$

Therefore, we can explicitly compute the stationary distribution as

$$\begin{bmatrix} P_{\mathrm{ON}}(c) \\ P_{\mathrm{OFF}}(c) \end{bmatrix} = \begin{bmatrix} \dfrac{\tau_{\mathrm{ON}}(c)}{\tau_{\mathrm{ON}}(c) + \tau_{\mathrm{OFF}}(c)} \\ \dfrac{\tau_{\mathrm{OFF}}(c)}{\tau_{\mathrm{ON}}(c) + \tau_{\mathrm{OFF}}(c)} \end{bmatrix}. \quad (11)$$

In Fig. 11 *B*, we plot the stationary probability $P_{\mathrm{OFF}}(c)$ of a TEA molecule not bound to the channel as a function of the TEA concentration. The solid line fitted through the points derived from τ_{ON} and τ_{OFF} (see Eq. 11) is fitted with an exponential function of the form, exp $(ac + b)$ with $a = -0.104$ and $b = -0.08$. With e denoting the elementary charge, the average channel current is $\bar{i}(c) = eN \times P_{\mathrm{OFF}}(c) + 0 \times P_{\mathrm{ON}}(c) = eNP_{\mathrm{OFF}}(c)$, since when the blocker is ''ON'' the channel is blocked. Here N denotes the number of K^+ ions that moves across the channel in one second in the absence of TEA. Thus, $P_{\mathrm{OFF}}(c)$ is proportional to the average current $\bar{i}(c)$. It can be seen from Fig. 11 *B* that $P_{\mathrm{OFF}}(c)$ decays exponentially as the concentration c of TEA is increased. A similar exponential decay has been experimentally reported for the KcsA channel (5) (see Fig. 9).

A similar argument can be made for a random sequence of off-times and on-times as a function of the applied voltage. The depth of the well and the TEA concentration used for this series of analysis are, respectively, 13 kT and 3.2 mM. In this case, off-time τ_{OFF} (*solid circles*) and on-time τ_{ON} (*open circles*) are plotted in Fig. 12 *A* against applied potentials. The average time TEA stays bound to the channel, once it enters the binding pocket, increases as the applied potential increases, whereas the average time the channel remains

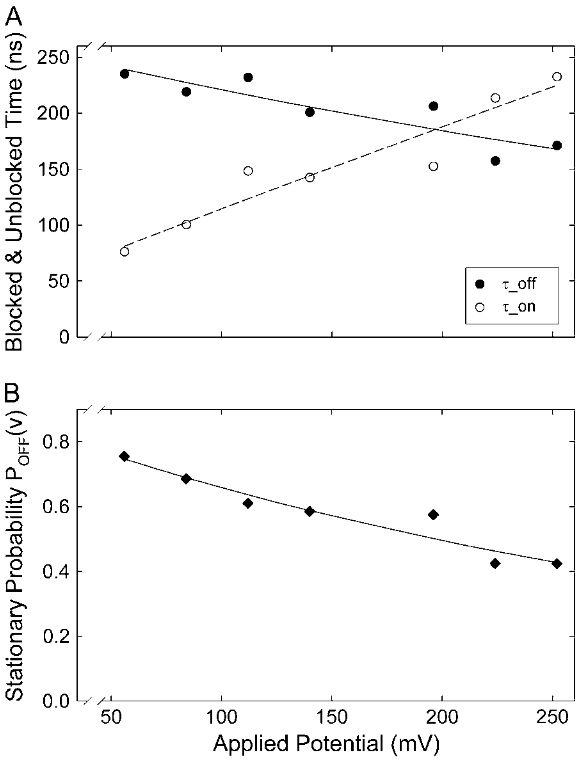

FIGURE 12 Voltage-dependent kinetics of TEA binding and unbinding. (*A*) The mean off-time τ_{OFF} (*V*) (*solid circles*) and the mean on-time τ_{ON} (*V*) (*open circles*) are plotted against applied potentials. (*B*) The stationary probability P_{OFF} of a TEA molecule being not bound to the channel is plotted against applied potentials.

unbound from the molecule decreases with an increasing applied potential. Once again, all random sequences obtained from BD simulations are shown to be exponentially distributed using the Anderson-Darling test. In Fig. 12 *B*, the $P_{OFF}(V)$ is fitted with the following two exponential functions: $\exp(-0.003V$ and $-0.133)$, where V is in mV.

DISCUSSION

For this study, we approximated the shape of TEA as a sphere with a radius of either 2.3 Å or 3.4 Å. Ideally, the molecule should be represented as an oblate spheroid whose long and short axes correspond to 2.3 and 4.6 Å. To incorporate spherically asymmetrical molecules as rigid bodies into the BD algorithm, we would need to follow, in addition to their translational steps, the rotational motions using unbiased operators for finite rotations (34). We should also need to determine the diffusion coefficient for rotational motions and may have to incorporate a hydrodynamic interaction term into the diffusion tensor (35). For this preliminary study, however, we use a simplified, spherical TEA model, deferring the more realistic representation of the molecule to a future project.

The stabilization of TEA by the four tyrosine residues in KcsA is likely to arise either from the hydration forces (9,10) or from the attractive interaction between a TEA molecule and the quadrupolar moment of the aromatic ring (3,11). Because in Brownian dynamics water molecules are not explicitly simulated, the interaction originating from the hydration force is not taken into account. Similarly, forces stemming from electrostatic interactions between a charged particle and quadrupolar moments are not calculated in our algorithm. We therefore implicitly account for these forces by incorporating in the BD algorithm the free energy profile obtained from molecular dynamics, so that each TEA molecule in the reservoir sees, in addition to all other attractive and repulsive forces it encounters, the attractive force generated by the tyrosine residues near the entrance of the selectivity filter. The so-called potential of mean force derived from umbrella sampling calculations using the weighted histogram analysis method (36) is in fact a one-dimensional free energy profile. For use in BD, it should first be converted into a one-dimensional potential energy profile and then into a three-dimensional free energy profile. The interrelationships between these profiles are briefly summarized in Appendix 1.

By grafting into BD the additional force encountered by TEA in the simulation assembly, we uncover several subtle features of its mechanism of blockade. First, we determine the precise depth of the free energy profile external TEA has to encounter to reproduce the experimentally determined inhibitory constant (Figs. 6 and 9). We show that the depth of the energy-well has to be somewhat deeper than that calculated from molecular dynamics (9) to account for the experimental measurements. Secondly, the affinity to external TEA block also depends on the applied potential (Fig. 7) and, to a lesser extent, the ionic concentration in the outer reservoirs (Fig. 8). At a fixed applied potential, the current decreases exponentially with an increasing TEA concentration. Likewise, with a fixed TEA concentration, the percentage of inhibition relative to the control current increases as the applied potential increases. Thus, an inhibitory constant k_i derived at a fixed potential with one ionic concentration may not hold true for different experimental conditions, as noted previously by Eisenberg (37). Thirdly, our analysis of the sequences of blocking events reveals that binding and unbinding of TEA to the binding pocket is a first-order Markovian process. The transition rate for TEA binding increases steeply with the concentration, whereas that for unbinding remains invariant of the concentration (Fig. 11). The transition rate for binding and unbinding depends similarly on the applied potential (Fig. 12).

The depth of the well from the free energy profile calculated from molecular dynamics is 4.5 kcal/mol or 7.5 kT (9). The binding energy computed by Luzhkov and Åqvist (10) using an automated docking approach is slightly lower, ranging from 3.3 to 3.9 kcal/mol. From the one-dimensional free energy profile, we can directly estimate the probability of a TEA molecule found in the binding site, P_{bind}, and this in turn leads to an estimate for k_i (see Appendix 2). The value of the inhibitory constant with no applied potential estimated from the free energy profile of Crouzy et al. (9) is 23 mM. When the applied potential is increased from 0 mVA to 200 mV, the value of k_i shifts by 2.1 mM. Although the free energy profile obtained from molecular dynamics is unable to account for other subtle features of the dynamics of TEA blockade, it nevertheless provides an order-of-magnitude estimate of the inhibitory constant. More importantly, such a profile gives valuable information about the general shape of the three-dimensional free energy profile that needs to be incorporated into the Brownian dynamics algorithm. It is possible that the depth of the free energy profile calculated from molecular dynamics may become deeper once all four tyrosine residues are repositioned such that a TEA molecule in the binding site would interact with the faces of the aromatic side chains. Such an en face orientation is needed for the favorable cation-π electron interaction (11).

Yellen et al. (2) noted that internal TEA blocks a mutant *Shaker* channel, *ShIR*, at a submillimolar concentration. When threonine residues at position 441 are replaced with serines, the sensitivity to internally applied TEA is reduced by an order of magnitude. It thus appears that the *Shaker* K^+ channel possesses an internal TEA binding pocket similar to that found in the external vestibule. In contrast, the inhibitory constant for internally applied TEA for the KcsA K^+ channel is 22 mM (5). This value is close to the results of our simulation (Fig. 3). The suppression of the currents by internal TEA in our simulations is caused by the occlusion of the ion conducting pathway. The blocking molecule penetrates deeper inside of the pore as the applied potential is increased, thus making the effectiveness of blockade highly voltage-dependent (Fig. 2).

By making several simplifying assumptions, we have been able to deduce many of the salient features of internal and external TEA blockade in the KcsA K^+ channel. Here we have exploited the capability of BD to measure the current flowing across a biological ion channel to study how internally or externally applied TEA interacts with the permeation dynamics. By carrying out BD simulations in the KcsA potassium channels with TEA ions in KCl solutions, we show how the inward and outward currents change with an increasing concentration of TEA in the simulation assembly. From a series of such current-concentration curves constructed from different energy profiles with varying well-depths, we are able to infer the depth of the energy-well a TEA molecule needs to see to replicate the experimentally determined inhibitory constant for the TEA block. We also demonstrate that the attenuation of currents by TEA is dependent on other factors, such as the applied potential and ionic concentrations of potassium ions in the reservoirs. Moreover, by tabulating how long a TEA molecule stays bound in the binding site, we reveal the dynamics of binding and unbinding processes taking place in a fast timescale. The technique we introduce here can be fruitfully utilized in examining other K^+ channel models whose atomic coordinates are not yet determined. Any homology model of a K^+ channel constructed must account for its current-voltage-concentration profiles as well as the effects of quaternary ammonium ions on channel currents.

APPENDIX 1: ONE-DIMENSIONAL AND THREE-DIMENSIONAL FREE ENERGY PROFILES

The aim below is to determine the relationship between the three-dimensional potential model that can be used in BD and the one-dimensional free energy profile obtained by using molecular dynamics calculations (9). In BD, we model the three-dimensional potential as

$$U^{\mathrm{BD}}(x,y,z) = U^{\mathrm{PMF}}(z) + U^{\mathrm{SR}}(x,y,z), \qquad (12)$$

where $U^{\mathrm{PMF}}(z)$ is an arbitrary one-dimensional potential, and $U^{\mathrm{SR}}(x, y, z)$ models the short-range forces due to the channel walls. We wish to determine the potential $U^{\mathrm{PMF}}(z)$ so that the one-dimensional energy profile corresponding to Eq. 12 is equal to the one-dimensional free energy profile determined by molecular dynamics. As the free energy profile already includes an entropic component, we need to calculate the equivalent entropic component in BD. To do this, we must find the probability that the TEA resides within each cross-sectional area of the KcsA channel.

We start with the one-dimensional free energy profile obtained by using molecular dynamics. In one dimension, and at equilibrium, the probability of finding an ion per unit length is

$$P_{1\mathrm{d}}(z) = \frac{k_{1\mathrm{d}}}{L_0}\exp[-\beta G_{1\mathrm{d}}(z)], \qquad (13)$$

where $G_{1\mathrm{d}}(z) = G^{\mathrm{PMF}}(z)$ is the free energy in one dimension taken from Crouzy et al. (9), and $\beta = 1/kT$. Here, $k_{1\mathrm{d}}$ is a normalization constant, and L_0 is a reference length.

Even though profiles generated by WHAM analysis of molecular dynamics simulations are described as potentials of mean force, the nature of the analysis means that they reflect the probability of finding an ion at positions along the reaction coordinate, rather than the average (systematic) force along the reaction coordinate. In other words, they are free energy profiles, not potential energy profiles, and include an entropic component which depends on the effective cross-sectional area,

$$G^{\mathrm{PMF}}(z) = U^{\mathrm{PMF}}(z) - TS^{\mathrm{PMF}}(z), \qquad (14)$$

where $U^{\mathrm{PMF}}(z)$ is the potential energy, T is the absolute temperature, and $-TS^{\mathrm{PMF}}$ is the entropic component of the free energy.

In the case of hard boundaries, this entropic component is given by

$$TS^{\mathrm{PMF}}(z) = \beta^{-1}\ln(A^{\mathrm{PMF}}(z)/A_0), \qquad (15)$$

where $A^{\mathrm{PMF}}(z)$ is the cross-sectional area at each z position and $A_0 = (L_0)^2$ is a reference area. A larger area gives a larger entropy which leads to a smaller free energy and a greater probability (per unit length) of occupancy by an ion.

Now consider the three-dimensional potential model that can be used in BD. The probability of finding the TEA molecule per unit volume for any given cross section is

$$P_{3\mathrm{d}}(x,y,z) = \frac{k_{3\mathrm{d}}}{(L_0)^3}\exp[-\beta G_{3\mathrm{d}}(x,y,z)], \qquad (16)$$

where $G_{3\mathrm{d}} = U^{\mathrm{BD}}(x, y, z)$ is the free energy in three dimensions and $k_{3\mathrm{d}}$ is a normalization constant. Again, this is only valid at equilibrium, but the process of TEA binding and unbinding occurs at equilibrium.

The one-dimensional and three-dimensional probabilities can be related using

$$P_{1d}(z) = \int_{-\infty}^{\infty}\int_{-\infty}^{\infty} P_{3d}(x,y,z)dxdy. \tag{17}$$

By substituting from Eqs. 13 and 16, this gives

$$k_{1d}\exp[-\beta G_{1d}(z)] = (A_0)^{-1}\int_{-\infty}^{\infty}\int_{-\infty}^{\infty} k_{3d}\exp[-\beta G_{3d}(x,y,z)]dxdy. \tag{18}$$

After applying the natural log, Eq. 18 becomes

$$\ln(k_{1d}) - \beta G_{1d}(z) = \ln(k_{3d}) + \ln\left[(A_0)^{-1}\int_{-\infty}^{\infty}\int_{-\infty}^{\infty}\exp[-\beta G_{3d}(x,y,z)]dxdy\right]. \tag{19}$$

Since $G_{3d} = U^{BD}(x, y, z)$ from Eq. 12, Eq. 19 becomes

$$\ln(k_{1d}) - \beta G_{1d}(z) = \ln(k_{3d}) - \beta U^{PMF}(z) + \ln\left[(A_0)^{-1}\int_{-\infty}^{\infty}\int_{-\infty}^{\infty}\exp[-\beta U^{SR}(x,y,z)]dxdy\right]. \tag{20}$$

After rearranging terms,

$$\beta U^{PMF}(z) - \beta G_{1d}(z) = \ln(k_{3d}) - \ln(k_{1d}) + \ln\left[(A_0)^{-1}\int_{-\infty}^{\infty}\int_{-\infty}^{\infty}\exp[-\beta U^{SR}(x,y,z)]dxdy\right]. \tag{21}$$

The integral is an effective cross-sectional area, taking into account the short-range repulsive forces, rather than a hard boundary.

We assume that the channel has cylindrical symmetry such that

$$\beta U^{PMF}(z) - \beta G_{1d}(z) = \ln(k_{3d}) - \ln(k_{1d}) + \ln\left[(A_0)^{-1}\int_{0}^{\infty} 2\pi r\exp[-\beta U^{SR}(r)]dr\right]. \tag{22}$$

This assumption is justified since U^{SR}, the short-range forces from the BD force field, have cylindrical symmetry. Because $G_{1d}(z)$ is the result from Crouzy et al. (9), Eq. 22 represents the required correction needed to solve for the $U^{PMF}(z)$ for use in BD simulations.

Eq. 22 can be rewritten as

$$\beta U^{PMF}(z) - \beta G_{1d}(z) = k_G + \ln\left(\frac{A_R(z)}{(A_0)^{-1}}\right), \tag{23}$$

where

$$k_G = \ln(k_{3d}) - \ln(k_{1d}) \tag{24}$$

is the dimensionless free-energy offset, and

$$A_R(z) = \int_0^{\infty} 2\pi r\exp[-\beta U^{SR}(r,z)]dr \tag{25}$$

is the effective cross-sectional area, taking into account the short-range forces.

To make use of Eq. 23 in a BD simulation, we need to set a value for k_G so that the potential derived from the profile derived from molecular dynamics will match up with the potential from macroscopic electrostatics at the limit of the potential of mean force. We assume that at z_{max}, the extracellular limit of the free energy profile,

$$U^{PMF}(z_{max}) - G_{1d}(z_{max}) = 0; \tag{26}$$

so that, from Eq. 23,

$$k_G = -\ln\left(\frac{A_R(z_{max})}{A_0}\right). \tag{27}$$

APPENDIX 2: ESTIMATING THE INHIBITORY CONSTANT FROM PMF

It is possible to compute P_{bind}, the probability of a TEA being found in the binding site, directly from the one-dimensional free energy profile and the concentration of TEA in the reservoir. This in turn leads to an estimate for k_i, the concentration at half inhibition, by setting $P_{bind} = 1/2$.

We can estimate

$$P_{bind} = \int_{z_{min}}^{z_{max}} P_{1d}(z)dz, \tag{28}$$

$$= \frac{k_{1d}}{L_0}\int_{z_{min}}^{z_{max}}\exp[-\beta G_{1d}(z)]dz. \tag{29}$$

Since $G_{1d}(z) \equiv G^{PMF}(z)$, all we need in addition to the free energy profile to estimate P_{bind} from this formula is an estimate of k_{1d}.

From Eq. 23, we obtain

$$\exp\beta[U^{PMF}(z) - G_{1d}(z)] = \frac{k_{3d}}{k_{1d}}\frac{A_R(z)}{A_0}. \tag{30}$$

But $U^{PMF}(z_{max}) - G_{1d}(z_{max}) = 0$ from Eq. 26, so

$$k_{1d} = k_{3d}\frac{A_R(z_{max})}{A_0}. \tag{31}$$

We take $k_{3d}/V_0 = k_{RES}$, where $V_0 = (L_0)^3$, to be the TEA concentration in the reservoir in appropriate units (number density). Then from Eqs. 29 and 31

$$P_{bind} = \frac{k_{3d}}{V_0}A_R(z_{max})\int_{z_{min}}^{z_{max}}\exp[-\beta G_{1d}(z)]dz. \tag{32}$$

If $P_{bind} = 1/2$, then $k_i = k_{3d}/V_0$ and

$$k_i = \left[2A_R(z_{max})\int_{z_{min}}^{z_{max}}\exp[-\beta G_{1d}(z)]dz\right]^{-1}. \tag{33}$$

We thank Dan Gordon for his helpful comments on the manuscripts.

This work was supported by grants from the National Health & Medical Research Council of Australia. The calculations upon which this work is based were carried out using the Itanium2 processors of the Australian National University Supercomputing Facility.

REFERENCES

1. French, R. J., and J. J. Shoukimas. 1981. Blockage of squid axon potassium conductance by internal tetra-n-alkylammonium ions of various sizes. *Biophys. J.* 34:271–291.
2. Yellen, G., M. E. Jurman, T. Abramson, and R. MacKinnon. 1991. Mutations affecting internal TEA blockade identify the probable pore-forming region of a K^+ channel. *Science.* 25:939–942.
3. Heginbotham, L., and R. MacKinnon. 1992. The aromatic binding site for tetraethylammonium ion on potassium channels. *Neuron.* 8:483–491.

4. MacKinnon, R., and G. Yellen. 1990. Mutations affecting TEA blockade and ion permeation in voltage-activated K^+ channels. *Science*. 250:276–279.
5. Heginbotham, L., M. LeMasurier, L. Kolmakova-Partensky, and C. Miller. 1999. Single *Streptomyces lividans* K^+ channels: Functional asymmetries and sidedness of proton activation. *J. Gen. Physiol.* 114: 551–559.
6. Ikeda, S. R., and S. J. Korn. 1995. Influence of permeating ions on potassium channel block by external tetraethylammonium. *J. Physiol.* 486:267–272.
7. Immke, D., M. J. Wood, L. Kiss, and S. J. Korn. 1999. Potassium-dependent changes in the conformation of the Kv2.1 potassium channel pore. *J. Gen. Physiol.* 113:819–836.
8. Meuser, D., H. Splitt, R. Wagner, and H. Schrempf. 1999. Exploring the open pore of the potassium channel from *Streptomyces lividans*. *FEBS Lett.* 462:447–452.
9. Crouzy, S., S. Bernéche, and B. Roux. 2001. Extracellular blockade of K^+ channels by TEA: results from molecular dynamics simulations of the KcsA channel. *J. Gen. Physiol.* 118:207–217.
10. Luzhkov, V. B., and J. Åqvist. 2001. Mechanisms of tetraethylammonium ion block in the KcsA potassium channel. *FEBS Lett.* 495:191–196.
11. Ahern, C. A., A. L. Eastwood, H. A. Lester, D. A. Dougherty, and R. Horn. 2006. A cation-π interaction between extracellular TEA and an aromatic residue in potassium channels. *J. Gen. Physiol.* 128:649–657.
12. Consiglio, J., P. Andalib, and S. J. Korn. 2003. Influence of pore residues on permeation properties in the Kv2.1 potassium channel. Evidence for a selective functional interaction of K^+ with the outer vestibule. *J. Gen. Physiol.* 121:111–124.
13. Cha, A., and F. Bezanilla. 1997. Characterizing voltage-dependent conformational changes in the *Shaker* K^+ channel with fluorescence. *Neuron*. 19:1127–1140.
14. Yellen, G., D. Sodickson, T.-Y. Chen, and M. E. Jurman. 1994. An engineered cysteine in the external mouth of a K^+ channel allows inactivation to be modulated by metal binding. *Biophys. J.* 66:1068–1075.
15. Kiss, L., and S. J. Korn. 1998. Modulation of C-type inactivation by K^+ at the potassium channel selectivity filter. *Biophys. J.* 74:1840–1849.
16. Chung, S. H., J. B. Moore, L. Xia, L. S. Premkumar, and P. W. Gage. 1990. Characterization of single channel currents using digital signal processing techniques based on hidden Markov models. *Philos. Trans. R. Soc. Lond. B Biol. Sci.* B329:256–285.
17. Chung, S. H., V. Krishnamurthy, and J. B. Moore. 1991. Adaptive processing techniques based on hidden Markov models for characterizing very small channel currents in noise and deterministic interferences. *Philos. Trans. R. Soc. Lond. B Biol. Sci.* B334:243–284.
18. Chung, S. H., T. W. Allen, and S. Kuyucak. 2002. Conducting-state properties of the KcsA potassium channel from molecular and Brownian dynamics simulations. *Biophys. J.* 82:628–645.
19. Doyle, D. A., J. M. Cabral, R. A. Pfuetzner, A. Kuo, J. M. Gulbis, S. L. Cohen, B. T. Chait, and R. MacKinnon. 1998. The structure of the potassium channel: molecular basis of K^+ conduction and selectivity. *Science*. 280:69–77.
20. Li, S. C., M. Hoyles, S. Kuyucak, and S. H. Chung. 1998. Brownian dynamics study of ion transport in the vestibule of membrane channels. *Biophys. J.* 74:37–47.
21. Hoyles, M., S. Kuyucak, and S. H. Chung. 1998. Computer simulation of ion conductance in membrane channels. *Phys. Rev.* E58:3654–3661.
22. Chung, S. H., T. Allen, M. Hoyles, and S. Kuyucak. 1999. Permeation of ions across the potassium channels: Brownian dynamics studies. *Biophys. J.* 80:2517–2533.
23. Chung, S. H., T. W. Allen, and S. Kuyucak. 2002. Modeling diverse range of potassium channels with Brownian dynamics. *Biophys. J.* 83:263–277.
24. Hoyles, M., S. Kuyucak, and S. H. Chung. 1996. Energy barrier presented to ions by the vestibule of the biological membrane channel. *Biophys. J.* 70:1628–1642.
25. Stillinger, F. H., and A. Rahman. 1974. Improved simulation of liquid water by molecular dynamics. *J. Chem. Phys.* 60:1545–1557.
26. Guárdia, E., R. Rey, and J. A. Padró. 1991. Potential of mean force by constrained molecular dynamics: a sodium chloride ion-pair in water. *Chem. Phys.* 155:187–195.
27. Guárdia, E., R. Rey, and J. A. Padró. 1991. Na^+-Na^+ and Cl^--Cl^- ion pairs in water: mean force potentials by constrained molecular dynamics. *J. Chem. Phys.* 95:2823–2831.
28. Corry, B., T. W. Allen, S. Kuyucak, and S. H. Chung. 2001. Mechanisms of permeation and selectivity in calcium channels. *Biophys. J.* 80:195–214.
29. Hille, B. 2001. Ion Channels of Excitable Membranes. Sinauer Associates, Sunderland, MA.
30. Press, W. H., B. P. Flannery, S. A. Teukolsky, and W. T. Vetterling. 1993. Numerical Recipes. Cambridge University Press, New York.
31. Im, W., S. Seefeld, and B. Roux. 2000. A grand canonical Monte Carlo-Brownian dynamics algorithm for simulating ion channels. *Biophys. J.* 79:788–801.
32. Corry, B., M. Hoyles, T. W. Allen, M. Walker, S. Kuyucak, and S. H. Chung. 2002. Reservoir boundaries in Brownian dynamics simulations of ion channels. *Biophys. J.* 82:1975–1984.
33. Anderson, T. W., and D. A. Darling. 1952. Asymptotic theory of certain ''goodness-of-fit'' criteria based on stochastic process. *Ann. Math. Stat.* 23:193–212.
34. Beard, D. A., and T. Schlick. 2003. Unbiased rotational moves for rigid-body dynamics. *Biophys. J.* 85:2973–2976.
35. Ermak, D. L., and J. A. McCammon. 1978. Brownian dynamics with hydrodynamic interactions. *J. Chem. Phys.* 69:1352–1360.
36. Kumar, S., D. Bouzida, R. H. Swendsen, P. A. Kollman, and J. M. Rosenberg. 1992. The weighted histogram analysis method for free-energy calculations on biomolecules. I. The method. *J. Comput. Chem.* 13:1011–1021.
37. Eisenberg, R. S. 1996. Computing the field in proteins and channels. *J. Membr. Biol.* 150:1–25.